This is the peer reviewed author accepted manuscript (post print) version of a published work that appeared in final form in:

Han, Sensen, Wang, Pengcheng, Zhou, Yi, Meng, Qingshi, Aakyiir, Mathias, Ma, Jun 2022 'Flexible, mechanically robust, multifunctional and sustainable cellulose/graphene nanocomposite films for wearable human-motion monitoring', Composites Science and Technology, in press, pp. 1-8

This output may not exactly replicate the final published authoritative version for which the publisher owns copyright. It is not the copy of record. This output may be used for non-commercial purposes. This version is licensed under a Creative Commons CC-BY-NC-ND 4.0 license (http://creativecommons.org/licenses/by-nc-nd/4.0/).

The final definitive published version (version of record) is available at: https://doi.org/10.1016/j.compscitech.2022.109451

Persistent link to the UniSA Research Outputs Repository: https://researchoutputs.unisa.edu.au/11541.2/31305

General Rights

Copyright and moral rights for the publications made accessible in the UniSA Research Outputs Repository are retained by the authors and/or other copyright owners and it is a condition of accessing publications that users recognize and abide by the legal requirements associated with these rights.

- Users may download and print one copy for the purpose of private study or research.
- You may not further distribute the material or use it for any profit-making activity or commercial gain
- You may freely distribute the persistent link identifying the publication in the UniSA Research Outputs Repository

If you believe that this document breaches copyright, please contact us and provide details. We will remove access to the work immediately and investigate your claim.

Flexible, Mechanically Robust, Multifunctional and Sustainable Cellulose/Graphene Nanocomposite Films for Wearable Human-Motion Monitoring

Sensen Han[1], Pengcheng Wang[1], Yi Zhou[3], Qingshi Meng[1*],

Mathias Aakyiir[2], Jun Ma[2*]

[1] College of Aerospace Engineering, Shenyang Aerospace University, Shenyang 110136, China

[2] UniSA STEM and Future Industries Institute, University of South Australia, Mawson Lakes, SA 5095, Australia.

[3] Dyson School of Design Engineering, Imperial College London, London SW7 2DB, United Kingdom

[*]Corresponding Author: Qingshi Meng and Jun.Ma

Email: mengqingshi@hotmail.com and Jun.Ma@unisa.edu.au

Sensen Han and Pengcheng Wang contributed equally to this article.

Abstract

The recent sensing technology development for flexible electronics has led to applications in intelligent robots, human-machine interfaces and health monitoring. However, it is challenging to combine ultra-light weight, high durability and flexibility, rapid response and simple fabrication within a single sensor. We herein report a cost-effective, sustainable preparation route for such a sensor, through (i) self-assembling cellulose nanofibers (CNFs) and *graphene nanoplatelets modified by Triton X-100 (X-100-GNPs)* and (ii) simply filtrating the mixture. *X-100-GNPs were found to relatively uniformly*

disperse in the CNF matrix due to strong interfacial interactions. A nanocomposite film containing 23.76 vol% of GNPs displayed an electrical conductivity of 9.67 S/cm with mechanical robustness – Young's modulus of 6.18 GPa and tensile strength of 173 MPa. The efficient conductive GNP network provided the nanocomposite film sensors with integration of rapid response *(61 ms with 1.5 KPa)* and high flexibility, sensitivity and durability over 10,000 loading and unloading cycles *at 1 Hz within 0–0.5% tensile strain*. Used as a wearable strain sensor, the film demonstrated remarkable sensing capabilities in physiological signals, voice recognition, repression changes, muscle contraction and joint bending.

Key words: Graphene; Natural fibers; Nano composites

1. Introduction

As an increasingly important class of renewable, readily biodegradable and polymeric materials, cellulose is extracted from abundant natural fibers and has a one-dimensional morphological structure with an exceptional number of hydroxyl groups [1, 2]. Cellulose and its derivatives have been proposed for a wide range of applications including architecture, microelectronics, textile and medicine. Due to low cost, light weight, satisfactory thermal stability, eco-friendliness and biocompatibility, cellulose was used as a matrix for flexible sensors [3]. Since cellulose nanofibers (CNFs) are electrically insulating, they are often compounded with conducting particles [4, 5], in particular carbon nanomaterials [6, 7], which represents an advance over carbon-only flexible electronics [8, 9].

Within this context, graphene is known for exceptional mechanical properties, specific surface area and electrical conductivity [10], which makes it suitable for the development of flexible strain sensing devices [11-13]. Therefore, graphene oxide (GO) has been developed from graphite by heavy oxidation. Although thermal reduction removes oxygen, defects still remain in GO, leading to orders of magnitude lower electrical conductivity and nearly 75% of reduction in stiffness [14].

Solution-processable graphene nanoplatelets (GNPs, each platelet 2–5 nm in thickness) have been developed by combining thermal shock and ultrasonication [15-18]; they are different to GO in terms of (i) potential low production cost estimated at 10–20 US$/kg in comparison with 30 US$/kg for GO excluding the reduction cost, (ii) high structural integrity as evidenced by a Raman I_D/I_G ratio of ~0.07 in comparison with ~1.0 for reduced GO [19] and thus no reduction is needed and (iii) maximum resemblance of stiffness and electrical (1460 S/cm) and thermal conductivities to graphene. What's more, the GNP surface can be covalently modified by long-chain, amine-end surfactants [20, 21].

In contrast with carbon black nanoparticles, GNPs have been used in flexible strain sensors, which exhibit satisfactory mechanical performance, sensitivity, response speed, resolution and durability [22-25]. However, it is a great challenge to compound hydrophilic CNFs with hydrophobic GNPs to produce an electrically conductive, mechanically resilient nanocomposite film for sensing applications. A hypothesis made herein was that through proper surface modification, GNPs would form a network with a

CNF matrix thus offering excellent mechanical properties and electrical conductivity for sensing human motions.

In this scenario, we report a facile, cost-effective and sustainable route to preparing eco-friendly, mechanically robust and highly flexible CNF/X-100-GNP nanocomposite films as strain sensors, which can readily distinguish various strain levels of human motion signals. Briefly, GNPs are modified by Triton X-100, followed by mixing with CNFs and filtration to obtain CNF/X-100-GNP nanocomposite films. The microstructure, mechanical properties and multiple sensing applications of the films are investigated. The conductive GNP network within the CNF matrix responds to various strain and temperature changes.

2. Experimental

2.1 Materials. All of the experimental materials and characterization are shown in *Section 4* of the Supporting Information. *Our optimized preparation for aqueous X-100-GNP suspensions is described as below: 50 mg of GNPs and 0.2 ml of Triton X-100 were added to 200 ml of distilled water in a beaker, followed by mechanical stirring for 80 min and ultrasonication below 20 °C for 1 h. Ultrasonication at a relatively low temperature proved to promote the dispersion of nanoparticles in solvent [26]. This produced aqueous X-100-GNP suspension.*

2.2 Nanocomposite film sensor. Figure 1 illustrates the preparation of a CNF/X-100-GNP nanocomposite film sensor. The X-100-GNPs suspension was mixed with as-received CNFs in DI water (weight ratio 1:5), stirred at 500 rpm for 30 min and then

ultrasonicated for 60 min below 20℃. The resultant mixture was filtrated to obtain a flexible nanocomposite film. After rinsing with ethanol (99.9% in purity), the film was peeled off from the filtration membrane and dried, followed by mechanical pressing between two glass slides under 30 MPa for 5 min at room temperature. Copper wires of 2 μm in diameter were connected to both ends of the film with silver paste, to produce external electrodes. PDMS was used to seal the film ends by curing (80 ℃, 30 min), which were subsequently wrapped with adhesive tape. The wearable sensors were then placed on target locations of a human body with medical tape. The dimensions of the film sensors attached to the chest, knuckle, throat and wrist were 3×3, 2×4, 2×3 and 2×4 cm, respectively.

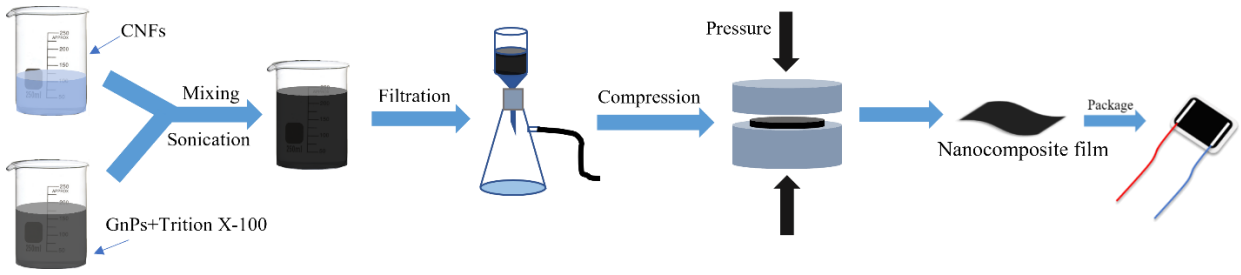


Figure 1 Schematic for preparation of a cellulose nanofibre/graphene nanocomposite film sensor

3. Result and discussion

3.1 Graphene nanoplatelets. Figure 2(a) contains a typical transmission electron microscopy (TEM) image of graphene nanoplatelets (GNPs), where a giant plate-like piece is found; the piece consists of a few layers of graphene stacked. Most GNPs were measured to be 2–4 nm in thickness in Figure S1 in the Supporting Information, in agreement with previous studies [27-29], indicating that each nanoplatelet in average consists of 2–4 graphene layers. A region was randomly selected to study electron diffraction (ED) pattern in Figure 2(b). *Its ED pattern shows a typical six-fold symmetry, which is usually expected for highly crystalline structure confirming that the region contains a few sheets of monolayer graphene.* This refers to that GNPs possess ultra-thin crystalline structure and each contains a small number of graphene layers, corresponding to the high electrical conductivity of 1,460 S/cm reported before [30].

The XRD patterns of GNPs and the graphite intercalation compound (GIC) are shown in Figure 2(c). A GIC is known for retaining layered structure, and it exhibits an exceptionally strong diffraction pattern at 26.18°. In contrast, GNPs demonstrate a diffraction pattern at a similar 2θ angle, indicating a structure with an interlayer spacing of 0.3 nm, but the intensity is significantly reduced, which is explained by the preparation process of GNPs. In specific, GIC was converted into GNPs through thermal expansion and subsequent ultrasonication at a relatively low temperature. The significantly reduced diffraction intensity is mainly due to two reasons. First, GIC composes of stages, each of which contains few-layer graphene stacked; one stage would be a GNP; these stages are

separated by intercalants of alkaline, metal salts or others. Upon being heated to 700°C, the intercalants rapidly evaporate resulting in enormous pressure [31], which expands the GIC's volume over 200 times producing a loose, worm-like structure. Second, through ultrasonication, the expanded product (worm-like structure) delaminates into GNPs, resulting in (i) corrugation, voids and reduction in the lateral dimension, (ii) increase in layer spacing between stages or (iii) even complete exfoliation.

The structure and integrity of GNPs were investigated and compared to GIC by Raman spectroscopy. Both GIC and GNPs demonstrate obvious absorptions at 1340, 1585 and 2690 cm^{-1} in Figure 2(d) which correspond to D, G, and 2D bands, respectively. The intensity ratio of D to G band (I_D/I_G) is always used to evaluate the degree of structural integrity of the GIC and GNPs. This low I_D/I_G ratio (~0.07) indicates that GNPs possess high structural integrity, reflecting high electrical conductivity and mechanical properties. However, GIC shows an I_D/I_G ratio of ~0.25, because the intercalated chemicals and the oxygenated groups on the GNP edges and surface both contribute to the increased I_D.

Figure 2(e) contains FTIR spectra of GNPs and X-100-GNPs. The characteristic bands of GNPs, i.e. 1670 cm^{-1} and 3620 cm^{-1}, attribute to the presence of oxygen-containing groups. The absorption peaks at 3280, 3304 and 3620 cm^{-1} imply that X-100 molecules are grafted onto GNPs likely through physical interaction. Figure 2(f) contains TGA curves of GNPs and X-100-GNPs. From room temperature to 600 ℃, the mass loss values of GNPs and X-100-GNPs were 0.2 wt% and 4.9 wt%, respectively. By substituting TGA data into the formula in the Supporting Information, the grafting ratio of Triton-X-100

was calculated to be 4.9 wt%. The grafted molecules would bridge GNPs with the CNF matrix, thus promoting strong interfacial interactions. *In Figure S2 in the Supporting Information, we reported that the grafting ratio reduced with more washing times.*

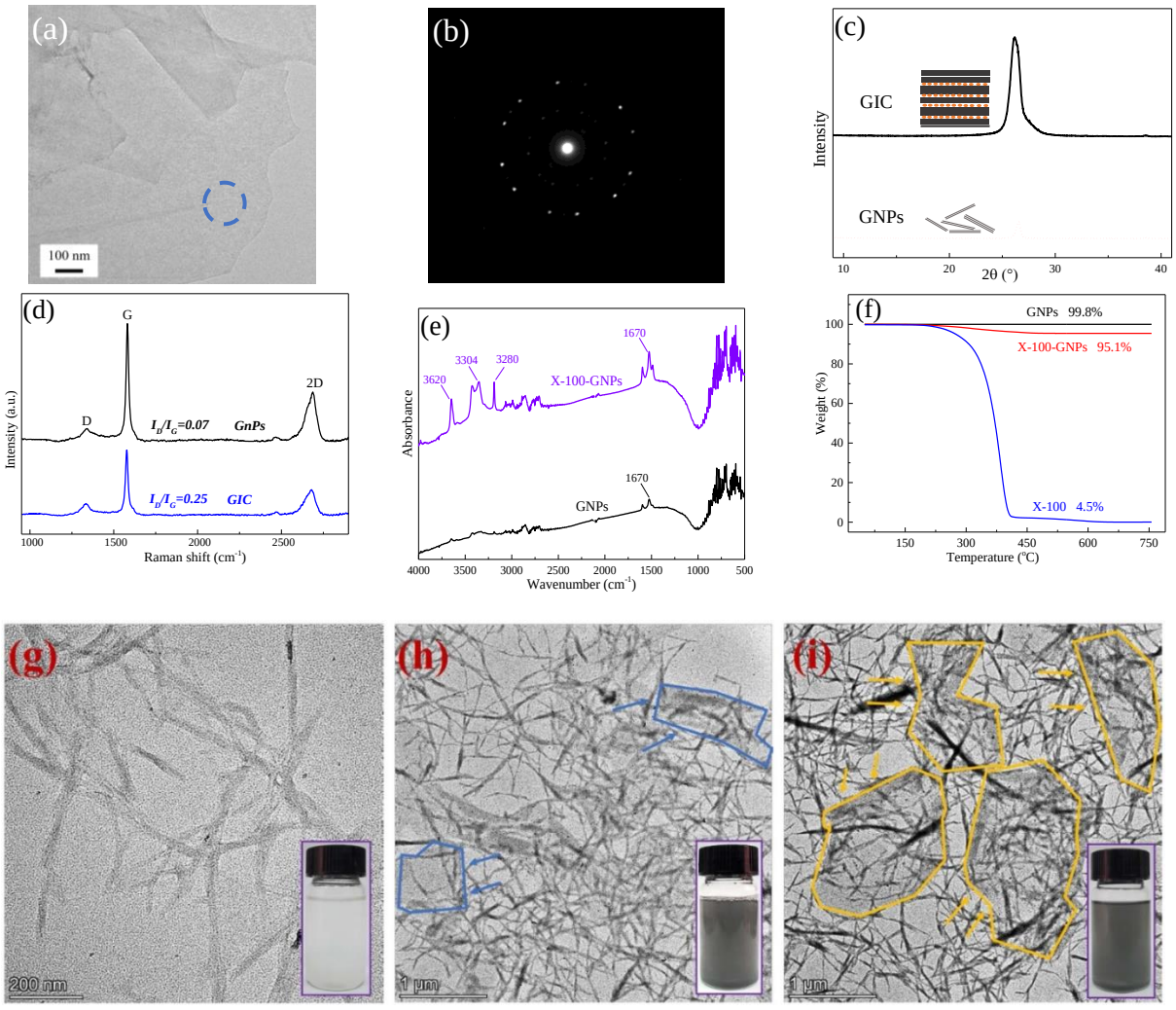


Figure 2 (a & b) TEM micrographs of graphene nanoplatelets (GNPs). Spectra of (c) XRD, (d) Raman, (e) FT-IR and (f) TGA. TEM micrographs of (g) neat CNFs, (h) CNF/X-100-GNP at 3.69 vol% and (i) CNF/X-100-GNP at 15.39 vol%.

In Table S1 in the Supporting Information, we converted wt% to vol% by ignoring the voids in the composites. Figure 2 (g-i) displays TEM micrographs of neat CNFs and the CNF/X-100-GNP nanocomposites. In Figure 2(g), CNFs have diameters of 5–20 nm and

length of 1–3 μm. The bottomright corner macroscopic image shows that CNFs stably disperse in water and that the suspension is transparent. This is explained by a fact that carboxyl and hydroxyl groups on CNF can provide strong electrostatic repulsion for stable dispersion in water [32]. Figure 2(h & i) reveals that CNFs are attached to the surfaces of GNPs (as pointed out by blue and yellow lines and arrows) and in turn these GNPs are well dispersed in the CNF matrix. This implies that through filtration, these suspensions would form nanocomposite films of satisfactory strength.

3.2 Morphology analysis of nanocomposite films. The top surface and cross-section of a CNF nanocomposite film containing 15.39 vol% of X-100-GNPs were examined by SEM (Figure 3). Since the top surface and cross-section of a neat CNF film are featureless as reported in previous research [33, 34], these are not included here. In Figure 3(a1–a3) displaying a rough top surface, we expected to see many scattered CNFs. On the contrary, no obvious CNFs are found even at a high magnification in Figure 3(a2). This is explained as (i) the modification and high flexibility of thin GNPs enable themselves to stay with CNFs or even wrap CNFs by the action of vacuum filtration (TEM, Figure2g-i) and (ii) the vacuum filtration and pressing processes further improve the combination between CNFs and X-100-GNPs. When the rough surface is further magnified in Figure 3(a3), voids are seen, as indicated by red circles. These voids would enable PDMS macromolecules to bolt into the nanocomposite film during the sensor preparation, to create a protection layer for sensing applications.

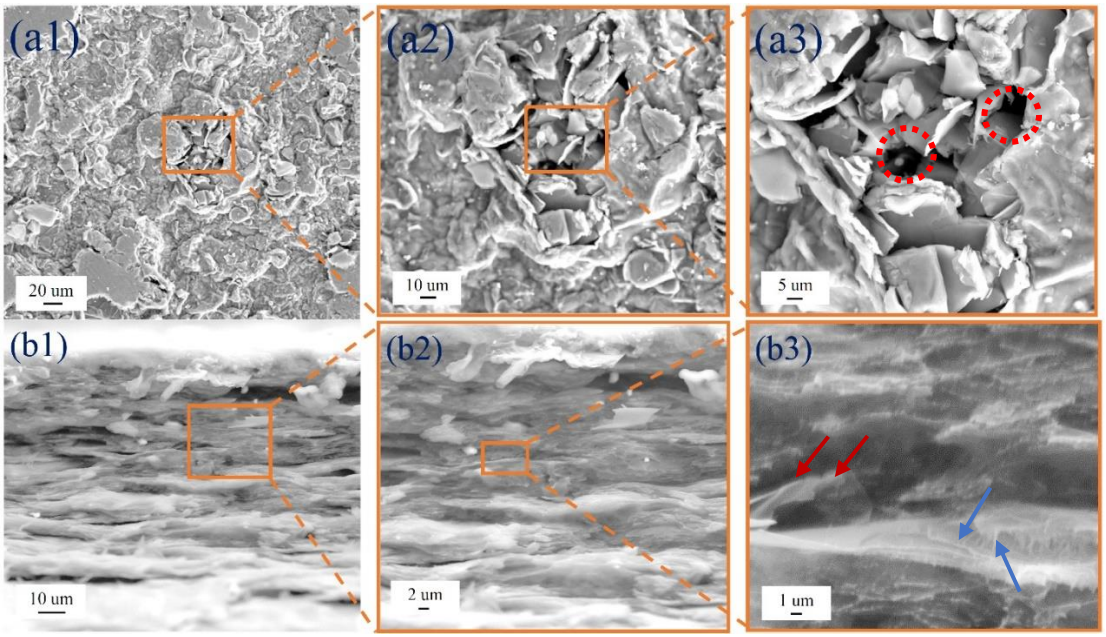


Figure 3 SEM micrographs of a cellulose nanofiber film containing 15.39 vol% of X-100-GNPs: (a) top surfaces and (b) fracture surfaces.

In Figure 3(b1), the film cross-section exhibits a compact layer-by-layer stacking structure due to both the directional flow induced by vacuum filtration and the mechanical compression. The distinctive morphology supports the increased modulus for the nanocomposite film in Figure 4. When a typical zone is magnified in Figure 3(b2), we cannot see a clear boundary, confirming a strong interface between CNFs and GNPs. This is mainly due to the effective interface modification and relatively uniform dispersion of GNPs (TEM, Figure 2(g-i)). The explanation is evidenced in Figure 3(b3) where many 1-dimensional CNFs (blue arrows) are intimately wrapped over 2D GNPs (red arrows). In conclusion, the nanocomposite film exhibits rough fracture surface, revealing strong interfacial adhesion and thus good compatibility between GNPs and CNFs. Such intimate and tightly packed structure corresponds to the high mechanical stiffness and electrical

conductivity in Figure 4.

3.3 Mechanical and electrical properties. Figure 4 contains tensile strength, Young's moduli and electrical conductivity of a CNF nanocomposite film containing 15.39 vol% of X-100-GNPs. Compared with the neat CNF film, the addition of X-100-GNPs has posed a significant effect on the mechanical properties and electrical behavior of the CNF matrix. In Figure 4(a), Young's modulus increases obviously, reaches a plateau at ~15.39 vol% of X-100-GNPs and then reduces. *The maximum modulus was measured to be 6.87 ± 0.35 GPa*, *representing a 29% improvement.* The introduction of rigid, two-dimensional thin nanosheets into a cellulose matrix can produce a stiffening effect. Actually, the enhanced moduli of the nanocomposite films are resulted from the surface modification of GNPs, which improves their compatibility with CNFs and leads to relatively uniform dispersion in the matrix. On the contrary, the tensile strength decreases slightly with increasing X-100-GNPs.

The opposite trends demonstrated by Young's modulus and tensile strength are explained below. Young's modulus is determined as the slope of the initial straight portion in a stress-strain graph, and in this study it was calculated using 0.002–0.100% strain. Tensile strength refers to the maximum stress, and it occurs at 5–10% strain herein. The introduction of rigid, two-dimensional nanosheets into a relatively soft matrix can produce an obvious stiffening effect at very low strains. However, GNPs would act as defects at high strains, leading to reduced strength.

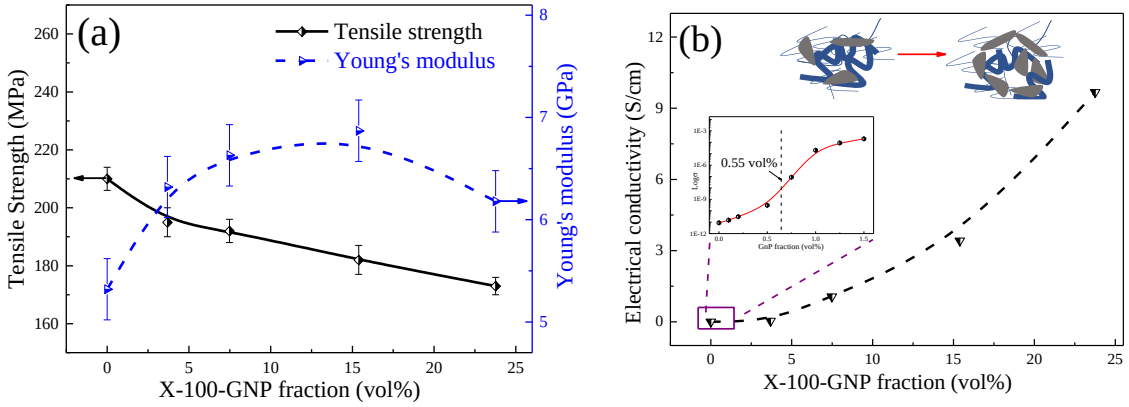


Figure 4 Cellulose/X-100-graphene nanocomposites: (a) mechanical properties and (b) electrical conductivity

Since cellulose is inherently electrically insulative, the incorporation of GNPs is expected to provide electrical conductivity. Figure 4(b) illustrates the electrical conductivity of the nanocomposite films as a function of X-100-GNPs. At low fractions (< 0.55 vol%), GNPs are far apart from each other within the CNF matrix, leading to an overall small increment of electrical conductivity. With increasing the X-100-GNP fractions, the inter-distance between GNPs is reduced, forming a rigid, rich global 3D network of X-100-GNPs for effective electron transfer. This explains why the nanocomposite film reaches an electrical conductivity of 9.67 S/cm at 23.76 vol% of X-100-GNPs. *Striking a balance between conductivity and mechanical resilience, the 15.39 vol% nanocomposite of 1.7 g/cm^3 in density was selected to investigate the piezoelectric sensing performance.*

3.4 Performance as a flexible sensor. Sensitivity, resolution, response time and reliability are the most important parameters to characterize a flexible strain sensor. Figure 5(a) shows $\Delta R/R_0$ of a nanocomposite film sensor under compression. As the compressive load augments to 2.5 KPa, $\Delta R/R_0$ decreases from 0 to –28%. 1 KPa can induce a $\Delta R/R_0$ change from 0 to –5%. Under compression, the interlayer spacing of the nanocomposite film decreases, resulting in more connections between graphene nanoplatelets (GNPs) in the 3D network paths and hence a decrease in the electrical resistance. Figure 5(b) presents the response time of the sensor. When it was loaded with 1.5 KPa, the response time was measured as 61 ms; upon removal of load, $\Delta R/R_0$ took 83 ms to rebound back to zero.

Linearity is a parameter describing how close a sensitivity graph is to a straight line (also called a linear regression plot), commonly denoted R^2. As one of the most important mechanical deformations, tensile strain is thoroughly studied in literature. The sensitivity of strain sensors is the slope of a sensitivity graph. A sensitivity graph for resistive strain sensors is the plot of relative resistance change (calculated from output data) vs. strain (calculated from input data).

In Figure 5(c), the nanocomposite film sensor exhibits a nearly linear electrical response to tensile strain. By conducting linear regression analysis for the testing data, a fitted function with $R^2 = 0.99894$ for the sensitivity graph in Figure 5(c) is found to be a third order polynomial function (eqn (1)), which can be used to obtain a gauge factor.

$$\frac{\Delta R}{R_0} = -0.63\varepsilon^3 + 2.97\varepsilon^2 - 0.3\varepsilon + 0.73 \quad (1)$$

A gauge factor (GF) or the sensitivity is the slope of a sensitivity graph. The gauge factor in this study is interpreted as the first derivative of eqn (1), resulting in:

$$GF = \frac{d\left(\frac{\Delta R}{R_0}\right)}{d\varepsilon} = -1.89\varepsilon^2 + 5.94\varepsilon - 0.3 \quad (2)$$

where ΔR is the electrical resistance change, R_0 is the original electrical resistance, and ε is the strain. The gauge factor in eqn (2) is not a constant number but an algebraic function. Then this equation was used to draw a graph of gauge factor vs. strain in Figure 5(d), which is a curve rather than a straight line. Such a methodology was first proposed by Qiu et al [35]. Substituting a strain of 3% into eqn (2) leads to a gauge factor of 9.2.

Calibration directly relies on the relationship between the input and output data, where a monotonic relationship (sensitivity graph) is needed. Figure 5(e) schematically explains how calibration was designed and executed for a resistive strain sensor. The original input is the strain occurred on the sensor, and the sensor converts the strain into electrical resistance. The resistance inputs into a calibration unit which is a specific electrical circuit designed by the Field Programmable Gate Array (FPGA) technology. In the unit, the resistance is interpreted as a relative strain which is the measured strain reading.

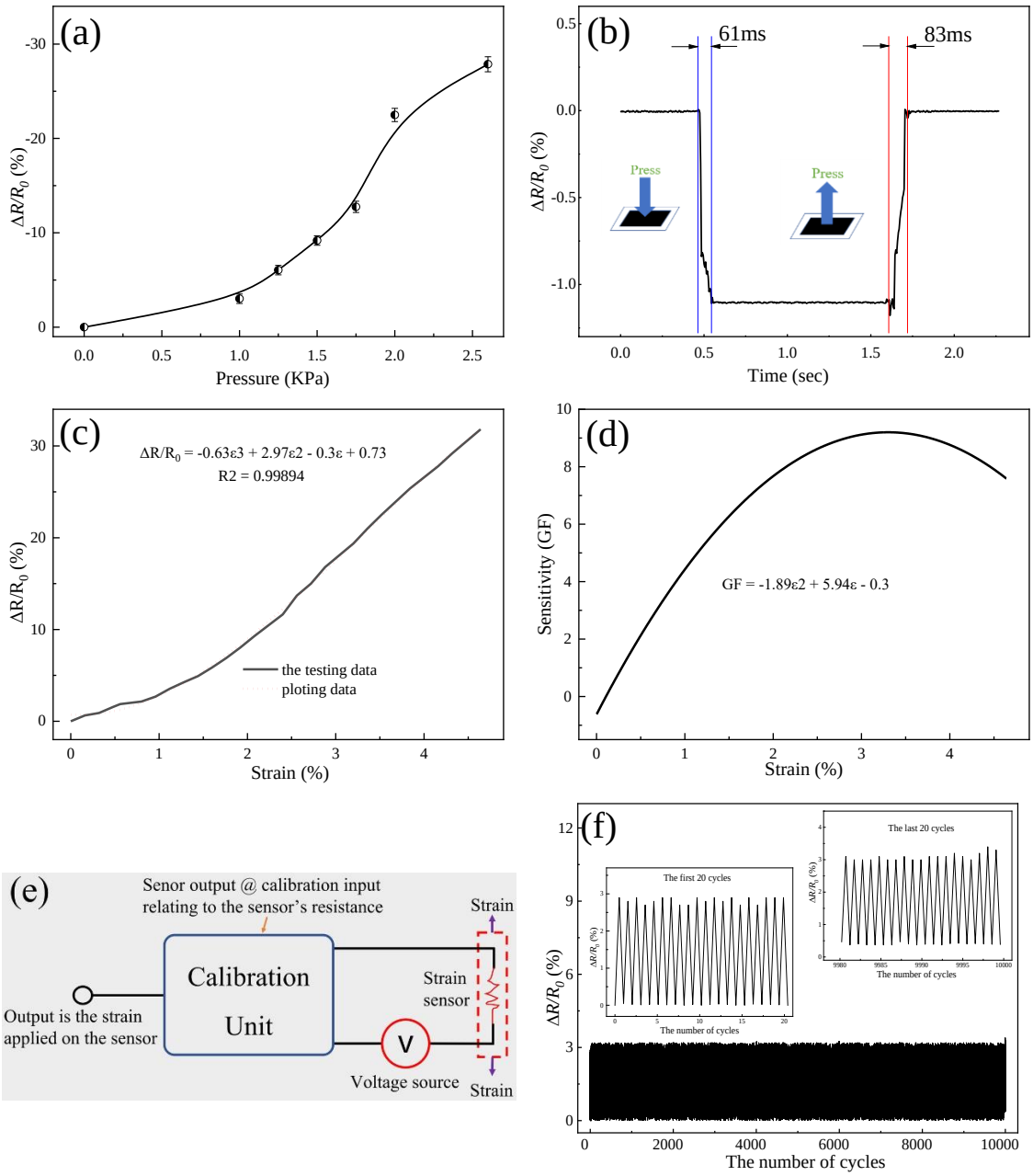


Figure 5 Piezoresistive responses of the nanocomposite film: (a) compressive loading, (b) response time, (c) resistance vs. strain, (d) sensitivity vs. strain, (e) schematic explanation of the calibration arrangement and (f) fatigue testing.

A flexible sensor is a sensing gauge which must be reliable. Reliability means that a strain sensor provides consistency of normal function without degradation. *Figure 5(f) shows $\Delta R/R_0$ evolution of a film sensor at 1 Hz for 10,000 cycles with tensile strains 0 to 0.5%*

at room temperature. Some irreversible detachment of conductive networks might cause a very minor increment of $\Delta R/R_0$, which was observed during the last 20 cycles. The high consistency between the first 20 cycles ($\Delta R/R_0$ from 0 to ~2.5%) and the last 20 cycles ($\Delta R/R_0$ from ~0.4% to ~3%) reveals the repeatability and reliability of the film sensor (Figure 5f insets). The exceptional cycling performance is explained from two aspects: (i) TEM and SEM demonstrated that the relatively uniform dispersion of X-100-GNPs in the CNF matrix and the strong interfacial adhesion between X-100-GNPs and CNFs due to the interface modification and (ii) the nanocomposite containing 15.39 vol% GNPs revealed modulus of 6.87 GPa, tensile strength of 182 MPa and fracture strain of ~6%, providing mechanical resilience for the exceptional cycling performance.

3.5 Physiological health monitoring. As a wearable electronic device, the flexible sensor was attached to human skin to detect various physiological signals, including heartbeat, pulse, respiration and body-temperature. Figure 6(a) discloses that the heartbeat pattern is more regular for a male athlete than for an ordinary man. Close observation reveals an $\Delta R/R_0$ of ~0.4% for the athlete in comparison with ~0.3% for the ordinary man. Figure 6(b) shows $\Delta R/R_0$ of 0.9% and heart rate of 120 times/min after the exercise, representing increments of 350% and 100%. The pulse with different physical exercises was also measured. Figure 6(c) illustrates an $\Delta R/R_0$ of ~0.40% for a male athlete and ~0.29% for an ordinary man. After physical exercise, the $\Delta R/R_0$ was measured as ~0.60% for the pulse rate with a frequency of 150 times/min, representing increments of 142% and 149%. Figure 6(e) shows the electrical signal responses to normal breathing and heavy breathing:

$\Delta R/R_0$ of ~0.2% for normal breathing and ~0.8% for heavy breathing. The change in $\Delta R/R_0$ can be attributed to the expansion of the nanocomposite film. The expansion would make neighboring GNPs further away and thus change the conductive pathways, resulting in higher electrical resistance.

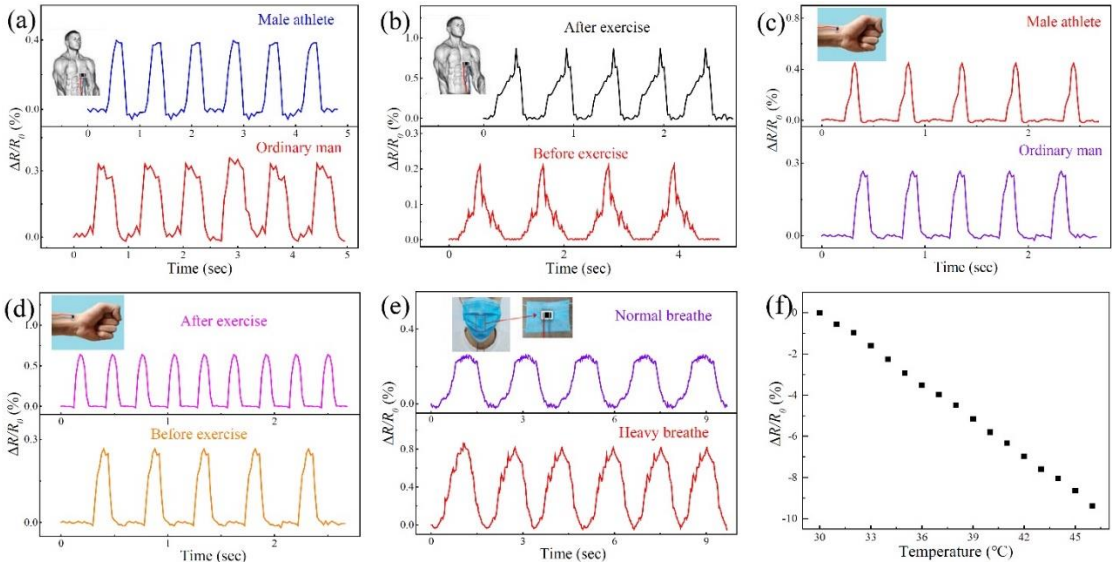


Figure 6 Detection of physiological signs: (a-b) heartbeat, (c-d) pulse, (e) breathe and (f) body temperature.

Precise measurement is essential to detect human body temperature which often reveals potential health issues. Figure 6(f) demonstrates that when temperature increases from 30 to 45 °C, $\Delta R/R_0$ decreases from 0 to −11.3%, demonstrating potential to be used as a new thermometer. The negative temperature coefficient can be attributed to GNPs' characteristic where upon thermal activation, electrons transfer from valence states to conduction states. A similar temperature-dependent resistant behavior has been reported for metallic carbon nanotubes, reduced graphene oxide and monolayer and bilayer graphene [36-38]. Uher et al.[39] have reported such unusual temperature-dependent

resistance in exfoliated graphite and the negative coefficient of resistivity was explained from activated behavior. The exact mechanisms need more in-depth investigation.

3.6 Voice recognition and facial expression changes. Hearing is realized when an eardrum converts the surrounding media changes into the nerve impulses. The flexible CNF/GNP nanocomposite film sensors have the potential to be used as artificial eardrums to transform sound information into electrical signals. When the flexible sensor was placed in an audio device as a sound signal collector, voice information was converted into electrical signals. In Figure 7(a-b), the graphs show different characteristics and repeated $\Delta R/R_0$ patterns when a speaker continuously pronounces letters and words. Pronouncing "A" results in a $\Delta R/R_0$ graph consisting of many dual peaks, clearly different to other graphs generated by pronouncing "B", "C" and "D". Similarly, when the speaker pronounces "Apple", "Banana", "Grape", "Orange" and "Peach", the sensor yields distinct $\Delta R/R_0$ waveforms in Figure 7(b). Noteworthy is that the peak pattern is nearly identical for each graph when a letter or word is repeatedly pronounced, which implies an excellent speech recognition capability. Hence, the nanocomposite film sensor should have an application prospect in human-machine interface as well as for pronunciation rehabilitation exercises.

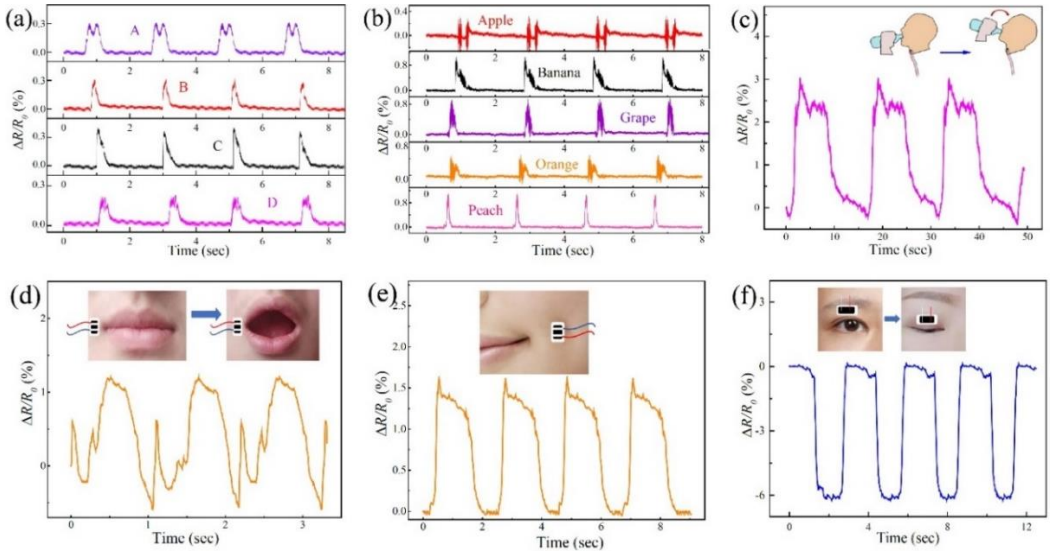


Figure 7 Detection of subtle deformation: (a & b) reading the words, (c) swallowing, (d) opening mouth, (e) dimple smile and (f) blinking.

Figure 7(c) illustrates sensing to the action of drinking water when a sensor is attached to the throat. Figure 7(d) shows a graph for detection of mouth opening or closing. When the sensor is used to detect smiling in Figure 7(e), $\Delta R/R_0$ increases by 1.5%; these four peaks are nearly identical, presenting repeatability or stability for the detection. When the sensor is attached with eyelids to detect blinking in Figure 7(f), $\Delta R/R_0$ reduces and increases regularly and simultaneously with blinking. In summary, the nanocomposite sensor in these applications yielded reproducible $\Delta R/R_0$ graphs. The peaks in each graph have nearly identical patterns. Each graph contains major and sharp minor peaks, indicating high sensitivity.

Muscle contraction monitoring and joint activities monitoring are available in *Sections 6 and 7* in the Supporting Information.

Conclusions

This study reported a facile, cost-effective and sustainable route for the development of a cellulose/graphene nanocomposite film, where the surface-modified graphene nanoplatelets (X-100-GNPs) were uniformly dispersed in the cellulose nanofiber (CNF) matrix. TEM and SEM micrographs demonstrated the strong interfacial adhesion and compatibility between X-100-GNPs and CNFs. The nanocomposite film containing 23.76 vol% of X-100-GNPs demonstrated an electrical conductivity of 9.67 S/cm with mechanical robustness. The nanocomposite's mechanical resilience and the efficient conductive GNP network led to integration of fast response and high flexibility, sensitivity and performance stability over 10,000 cycles. When used as a multifunctional sensor, the nanocomposite film revealed high sensitivity to different stimuli, e.g. mechanical (tensile strain, cyclic deformation and human motion) and environmental (temperature). The flexible, mechanically robust and multifunctional nanocomposite film sensors and its green fabrication processes are promising for advanced wearable electronics and bionics, with great potential in intelligent robots, human-machine interfaces, medical treatment and wearable health monitoring.

Competing Interest

The authors declare no competing interest.

Acknowledgments

JM acknowledges support from Australian Research Council (DP200101737).

Reference

[1] L. Li, B. Zhou, G. Han, et al., Understanding the effect of interfacial engineering on interfacial thermal resistance in nacre-like cellulose nanofiber/graphene film, Composites Science and Technology 197 (2020) 108229. https://doi.org/10.1016/j.compscitech.2020.108229

[2] T. Noguchi, M. Endo, K. Niihara, et al., Cellulose nanofiber/elastomer composites with high tensile strength, modulus, toughness, and thermal stability prepared by high-shear kneading, Composites Science and Technology 188 (2020) 108005. https://doi.org/10.1016/j.compscitech.2020.108005

[3] A. Rivadeneyra, A. Marín-Sánchez, B. Wicklein, et al., Cellulose nanofibers as substrate for flexible and biodegradable moisture sensors, Composites Science and Technology 208 (2021) 108738. https://doi.org/10.1016/j.compscitech.2021.108738

[4] S. Cui, P. Wei, L. Li, Preparation of poly (propylene carbonate)/graphite nanoplates-spherical nanocrystal cellulose composite with improved glass transition temperature and electrical conductivity, Composites Science and Technology 168 (2018) 63-73. https://doi.org/10.1016/j.compscitech.2018.09.012

[5] H.Y. Choi, T.-W. Lee, S.-E. Lee, et al., Silver nanowire/carbon nanotube/cellulose hybrid papers for electrically conductive and electromagnetic interference shielding elements, Composites Science and Technology 150 (2017) 45-53. https://doi.org/10.1016/j.compscitech.2017.07.008

[6] T.-W. Lee, S.-E. Lee, Y.G. Jeong, Carbon nanotube/cellulose papers with high

performance in electric heating and electromagnetic interference shielding, Composites Science and Technology 131 (2016) 77-87. https://doi.org/10.1016/j.compscitech.2016.06.003

[7] M. Gnanaseelan, Y. Chen, J. Luo, et al., Cellulose-carbon nanotube composite aerogels as novel thermoelectric materials, Composites Science and Technology 163 (2018) 133-140. https://doi.org/10.1016/j.compscitech.2018.04.026

[8] L. Ci, S.M. Manikoth, X. Li, et al., Ultrathick Freestanding Aligned Carbon Nanotube Films, Advanced materials 19(20) (2007) 3300-3303. https://doi.org/10.1002/adma.200602974

[9] D.N. Futaba, K. Hata, T. Yamada, et al., Shape-engineerable and highly densely packed single-walled carbon nanotubes and their application as super-capacitor electrodes, Nature materials 5(12) (2006) 987-994. https://doi.org/10.1038/nmat1782

[10] R.J. Young, I.A. Kinloch, L. Gong, et al., The mechanics of graphene nanocomposites: A review, Composites Science and Technology 72(12) (2012) 1459-1476. https://doi.org/10.1016/j.compscitech.2012.05.005

[11] L.-Q. Tao, K.-N. Zhang, H. Tian, et al., Graphene-Paper Pressure Sensor for Detecting Human Motions, ACS Nano 11(9) (2017) 8790-8795. https://doi.org/10.1021/acsnano.7b02826

[12] Y. Wang, L. Wang, T. Yang, et al., Wearable and highly sensitive graphene strain sensors for human motion monitoring, Advanced Functional Materials 24(29) (2014) 4666-4670. https://doi.org/10.1002/adfm.201400379

[13] S. Han, A. Chand, S. Araby, et al., Thermally and electrically conductive multifunctional sensor based on epoxy/graphene composite, Nanotechnology 31(7) (2020) 075702. https://doi.org/10.1088/1361-6528/ab5042

[14] D.R. Kauffman, A. Star, Graphene versus carbon nanotubes for chemical sensor and fuel cell applications, Analyst 135(11) (2010) 2790-2797. https://doi.org/10.1039/C0AN00262C

[15] G. Shi, S. Araby, C.T. Gibson, et al., Graphene Platelets and Their Polymer Composites: Fabrication, Structure, Properties, and Applications, Advanced Functional Materials 28(19) (2018). https://doi.org/10.1002/adfm.201706705

[16] S. Han, Q. Meng, S. Araby, et al., Mechanical and electrical properties of graphene and carbon nanotube reinforced epoxy adhesives: Experimental and numerical analysis, Composites Part A: Applied Science and Manufacturing 120 (2019) 116-126. https://doi.org/10.1016/j.compositesa.2019.02.027

[17] S. Han, Q. Meng, A. Chand, et al., A comparative study of two graphene based elastomeric composite sensors, Polymer Testing 80 (2019). https://doi.org/10.1016/j.polymertesting.2019.106106

[18] I.K. Zaman, H. C. Dai, J. Kawashima, N. Michelmore, A. Sovi, A. Dong, S. Luong, L. Ma, J., From carbon nanotubes and silicate layers to graphene platelets for polymer nanocomposites, Nanoscale 4(15) (2012) 4578-86. https://doi.org/10.1039/c2nr30837a

[19] B. Zhao, P. Liu, Y. Jiang, et al., Supercapacitor performances of thermally reduced graphene oxide, Journal of Power Sources 198 (2012) 423-427.

https://doi.org/10.1016/j.jpowsour.2011.09.074

[20] J. Ma, Q. Meng, A. Michelmore, et al., Covalently bonded interfaces for polymer/graphene composites, Journal of Materials Chemistry A 1(13) (2013) 4255. https://doi.org/10.1039/c3ta01277h

[21] J.M. Ma, Qingshi Zaman, Izzuddin Zhu, Shenmin Michelmore, Andrew Kawashima, Nobuyuki Wang, Chun H. Kuan, Hsu-Chiang, Development of polymer composites using modified, high-structural integrity graphene platelets, Composites Science and Technology 91 (2014) 82-90. https://doi.org/10.1016/j.compscitech.2013.11.017

[22] S. Han, Q. Meng, K. Xing, et al., Epoxy/graphene film for lifecycle self-sensing and multifunctional applications, Composites Science and Technology 198 (2020). https://doi.org/10.1016/j.compscitech.2020.108312

[23] S. Han, X. Zhang, P. Wang, et al., Mechanically robust, highly sensitive and superior cycling performance nanocomposite strain sensors using 3-nm thick graphene platelets, Polymer Testing 98 (2021). https://doi.org/10.1016/j.polymertesting.2021.107178

[24] G. Shi, Z. Zhao, J.H. Pai, et al., Highly sensitive, wearable, durable strain sensors and stretchable conductors using graphene/silicon rubber composites, Advanced Functional Materials 26(42) (2016) 7614-7625. https://doi.org/10.1002/adfm.201602619

[25] A. Qiu, P. Li, Z. Yang, et al., A path beyond metal and silicon:

polymer/nanomaterial composites for stretchable strain sensors, Advanced Functional Materials 29(17) (2019) 1806306. https://doi.org/10.1002/adfm.201806306

[26] I. Zaman, T.T. Phan, H.-C. Kuan, et al., Epoxy/graphene platelets nanocomposites with two levels of interface strength, Polymer 52(7) (2011) 1603-1611. https://doi.org/10.1016/j.polymer.2011.02.003

[27] S. Wang, M. Cao, G. Wang, et al., Effect of graphene nanoplatelets on water absorption and impact resistance of fibre-metal laminates under varying environmental conditions, Composite Structures 281 (2022) 114977. https://doi.org/10.1016/j.compstruct.2021.114977

[28] R. Wang, M. Aakyiir, A. Qiu, et al., Surface-tunable, electrically conductive and inexpensive graphene platelets and their hydrophilic polymer nanocomposites, Polymer 205 (2020) 122851. https://doi.org/10.1016/j.polymer.2020.122851

[29] S. Araby, Q. Meng, L. Zhang, et al., Electrically and thermally conductive elastomer/graphene nanocomposites by solution mixing, Polymer 55(1) (2014) 201-210. https://doi.org/10.1016/j.polymer.2013.11.032

[30] Q. Meng, J. Jin, R. Wang, et al., Processable 3-nm thick graphene platelets of high electrical conductivity and their epoxy composites, Nanotechnology 25(12) (2014) 125707. https://doi.org/10.1088/0957-4484/25/12/125707

[31] S. Araby, X. Su, Q. Meng, et al., Graphene platelets versus phosphorus compounds for elastomeric composites: flame retardancy, mechanical performance and mechanisms, Nanotechnology 30(38) (2019) 385703. https://doi.org/10.1088/1361-

6528/ab2a3d

[32] A. Isogai, T. Saito, H. Fukuzumi, TEMPO-oxidized cellulose nanofibers, nanoscale 3(1) (2011) 71-85. https://doi.org/10.1039/C0NR00583E

[33] N.D. Luong, N. Pahimanolis, U. Hippi, et al., Graphene/cellulose nanocomposite paper with high electrical and mechanical performances, Journal of Materials Chemistry 21(36) (2011) 13991-13998. https://doi.org/10.1039/C1JM12134K

[34] A. Kafy, K.K. Sadasivuni, A. Akther, et al., Cellulose/graphene nanocomposite as multifunctional electronic and solvent sensor material, Materials Letters 159 (2015) 20-23. https://doi.org/10.1016/j.matlet.2015.05.102

[35] A. Qiu, M. Aakyiir, R. Wang, et al., Stretchable and calibratable graphene sensors for accurate strain measurement, Materials Advances 1(2) (2020) 235-243. 10.1039/d0ma00032a

[36] A.D. Bartolomeo, M. Sarno, F. Giubileo, et al., Multiwalled carbon nanotube films as small-sized temperature sensors, Journal of Applied Physics 105(6) (2009) 064518. https://doi.org/10.1063/1.3093680

[37] Q. Shao, G. Liu, D. Teweldebrhan, et al., High-temperature quenching of electrical resistance in graphene interconnects, Applied Physics Letters 92(20) (2008) 202108. https://doi.org/10.1063/1.2927371

[38] Y. Chen, P. Pötschke, J. Pionteck, et al., Smart cellulose/graphene composites fabricated by in situ chemical reduction of graphene oxide for multiple sensing applications, Journal of Materials Chemistry A 6(17) (2018) 7777-7785.

https://doi.org/10.1039/C8TA00618K

[39] C. Uher, L.M. Sander, Unusual temperature dependence of the resistivity of exfoliated graphites, Physical Review B 27(2) (1983) 1326-1332. https://link.aps.org/doi/10.1103/PhysRevB.27.1326

List of Figure Caption

Figure 1 Schematic of fabrication of a cellulose/graphene nanocomposite film sensor.

Figure 2 Characterization of graphite intercalation compound and graphene nanoplatelets (GNPs): (a) TEM of GNPs; (c) XRD patterns, (d) Raman spectra, (e) FTIR spectra and (f) TGA. TEM images of the solution: (g) neat CNFs; (h) 3.69 vol% and (i) 15.39 vol% CNF/X-100-GNP.

Figure 3 SEM images of the 15.39 vol% Cellulose/X-100-Graphene film: (a) top surfaces and (b) fracture surfaces.

Figure 4 Cellulose/X-100-Graphene nanocomposite: (a) mechanical properties and (b) electrical conductivity.

Figure 5 Piezoresistive responses of the cellulose/graphene nanocomposite film: (a) compressive loading, (b) response time, (c) tensile strain and (d) fatigue testing.

Figure 6 Detection of physiological signs: (a-b) heartbeat, (c-d) pulse, (e) breathe and (f) body temperature.